Supporting Information

Programming magnetization dynamics in a Dy-croconic acid system

Yue Yang,[a] Xue-Ying Shao,[a] Jian-Xu Pan,[a] Xiao-Fang Dong,[a] Shen Wang,[a] Yu-Lu Liang,[a] Yi-Quan Zhang,*[c] Yu-Xia Wang*[a,b] and Peng Cheng*[a]

[a]Department of Chemistry, Frontiers Science Center for New Organic Matter, State Key Laboratory of Advanced Chemical Power Sources, and Haihe Laboratory of Sustainable Chemical Transformations (Tianjin), College of Chemistry, Nankai University, Tianjin 300071, China

[b]Tianjin Key Laboratory of Structure and Performance for Functional Molecules, College of Chemistry, Tianjin Normal University, Tianjin 300387, China

[c]Ministry of Education Key Laboratory of NSLSCS, School of Physical Science and Technology, Nanjing Normal University, Nanjing 210023, China

* zhangyiquan@njnu.edu.cn
* wangyuxia@tjnu.edu.cn
* pcheng@nankai.edu.cn

1. Structures and Crystal Data

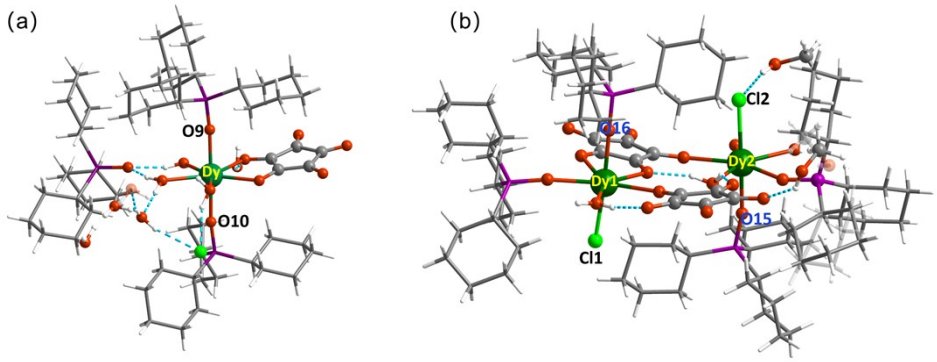

Fig. S1 (a) Complete crystal structure of **DyCA**. (b) Complete crystal structure of the asymmetric unit in **$[Dy_2CA_2]_n$**. Color scheme: green Dy, red O, grey C, purple P, light green Cl.

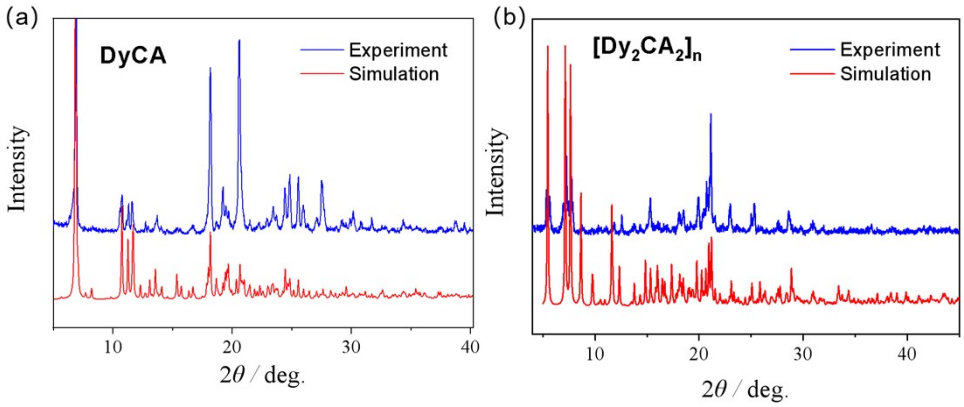

Fig. S2 Powder-XRD patterns of **DyCA** (a) and **$[Dy_2CA_2]_n$** (b), the blue lines are the experimental values and the red lines are the simulated values.

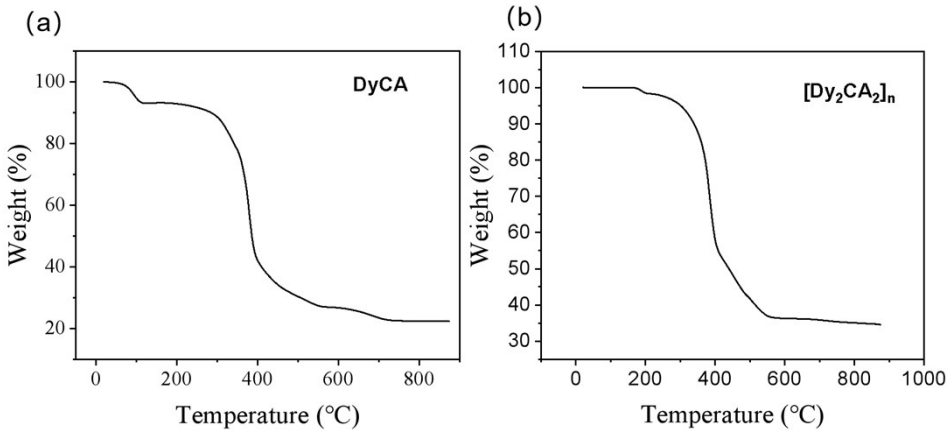

Fig. S3 TG curve of **DyCA** (a) and **$[Dy_2CA_2]_n$** (b).

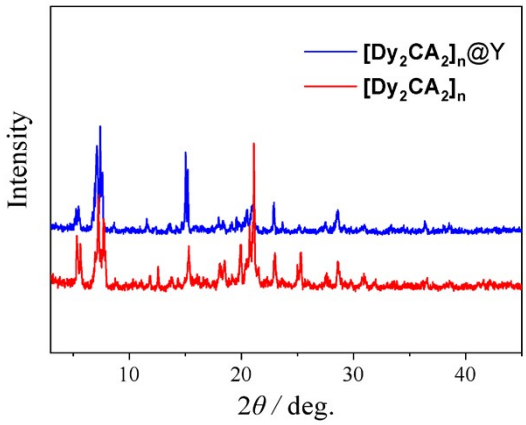

Fig. S4 Powder-XRD patterns of $[Dy_2CA_2]_n$ and $[Dy_2CA_2]_n$@Y. The blue line representing the magnetically diluted sample and red line representing the sample before dilution.

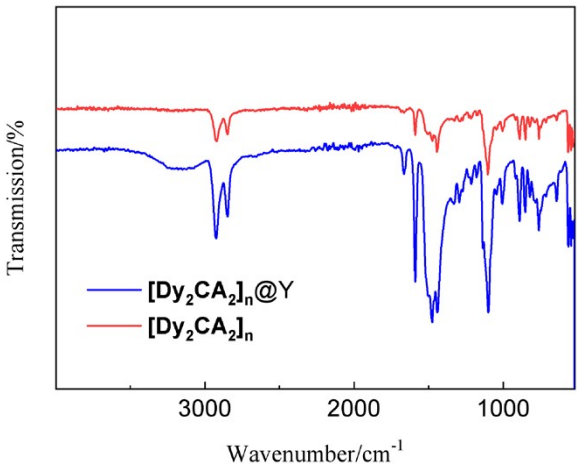

Fig. S5 Infrared spectra of $[Dy_2CA_2]_n$ and $[Dy_2CA_2]_n$@Y. The blue line representing the magnetically diluted sample and red line representing the sample before dilution.

Table S1 Crystallographic data and refinement parameters of **DyCA.**

	DyCA
formula	$C_{59}H_{111}ClDyO_{14}P_3$
fw	1335.33
temp(K)	100.00(10)
cryst system	Triclinic
space group	$P\bar{1}$
a(Å)	15.2125(4)
b(Å)	15.5239(4)
c(Å)	16.9589(5)
α(deg)	107.052(2)
β(deg)	94.261(2)
γ(deg)	117.435(3)
V(Å^3)	3293.17(18)
Z	2
Dc (g·cm^{-3})	1.347
Limiting indices	-17≤h≤18, -19≤k≤18, -20≤l≤21
μ(mm^{-1})	7.604
R_{int}	0.0456
GOOF	1.029
R_1	0.0458
wR_2	0.1026
$\triangle\rho_{max}$ (e Å^{-3})	1.863
$\triangle\rho_{min}$ (e Å^{-3})	-1.831
CCDC	2502518

$R_1 = \sum||Fo| - |Fc||/\sum|Fo|$; $wR_2 = [\sum w(Fo^2 - Fc^2)^2/\sum w(Fo^2)^2]^{1/2}$

Table S2 Crystallographic data and refinement parameters of **$[Dy_2CA_2]_n$**.

	$[Dy_2CA_2]_n$
CCDC	2502521
formula	$C_{84}H_{144}Cl_2Dy_2O_{18}P_4$
fw	1961.76
temp(K)	120.00(10)
cryst system	Monoclinic
space group	*I*2/*a*
a(Å)	33.7159(4)
b(Å)	10.76120(10)
c(Å)	51.6078(8)
α(deg)	90
β(deg)	106.692(2)
γ(deg)	90
V(Å^3)	17935.5(4)
Z	8
Dc (g·cm^{-3})	1.453
Limiting indices	-42≤h≤42, -13≤k≤11, -65≤l≤61
μ(mm^{-1})	10.550
R_{int}	0.0373
GOOF	1.004
R_1	0.0454
wR_2	0.1153
$\triangle\rho_{max}$ (e Å^{-3})	0.786
$\triangle\rho_{min}$ (e Å^{-3})	-1.105

$R_1 = \sum||Fo| - |Fc||/\sum|Fo|$; $wR_2 = [\sum w(Fo^2 - Fc^2)^2/\sum w(Fo^2)^2]^{1/2}$

Table S3 Detailed Continuous Shape Measures of **DyCA** at 100 K obtained by SHAPE.

DyCA							
Structure [ML_7]	HP-7	HPY-7	PBPY-7	COC-7	CTPR-7	JPBPY-7	JETPY-7
Shape	D_{7h}	C_{6v}	D_{5h}	C_{3v}	C_{2v}	D_{5h}	C_{3v}
Deviation value	33.167	25.126	0.195	7.310	5.437	2.802	23.779

HP-7 = Heptagon (D_{7h}); HPY-7 = Hexagonal pyramid (C_{6v}); PBPY-7 = Pentagonal bipyramid (D_{5h}); COC-7 = Capped octahedron (C_{3v}); CTPR-7 = Capped trigonal prism (C_{2v}); JPBPY-7 = Johnson pentagonal bipyramid J13 (D_{5h}); JETPY-7 = Johnson elongated triangular pyramid J7 (C_{3v})

Table S4 Detailed Continuous Shape Measures of **$[Dy_2CA_2]_n$** at 120K obtained by SHAPE.

$[Dy_2CA_2]_n$_Dy1							
Structure [ML_7]	HP-7	HPY-7	PBPY-7	COC-7	CTPR-7	JPBPY-7	JETPY-7
Shape	D_{7h}	C_{6v}	D_{5h}	C_{3v}	C_{2v}	D_{5h}	C_{3v}
Deviation value	35.255	25.357	0.449	7.046	5.728	4.567	24.038
$[Dy_2CA_2]_n$_Dy2							
Structure [ML_7]	HP-7	HPY-7	PBPY-7	COC-7	CTPR-7	JPBPY-7	JETPY-7
Shape	D_{7h}	C_{6v}	D_{5h}	C_{3v}	C_{2v}	D_{5h}	C_{3v}
Deviation value	34.036	24.872	0.515	6.459	4.809	4.337	23.382

HP-7 = Heptagon (D_{7h}); HPY-7 = Hexagonal pyramid (C_{6v}); PBPY-7 = Pentagonal bipyramid (D_{5h}); COC-7 = Capped octahedron (C_{3v}); CTPR-7 = Capped trigonal prism (C_{2v}); JPBPY-7 = Johnson pentagonal bipyramid J13 (D_{5h}); JETPY-7 = Johnson elongated triangular pyramid J7 (C_{3v})

2. Magnetic Measurements

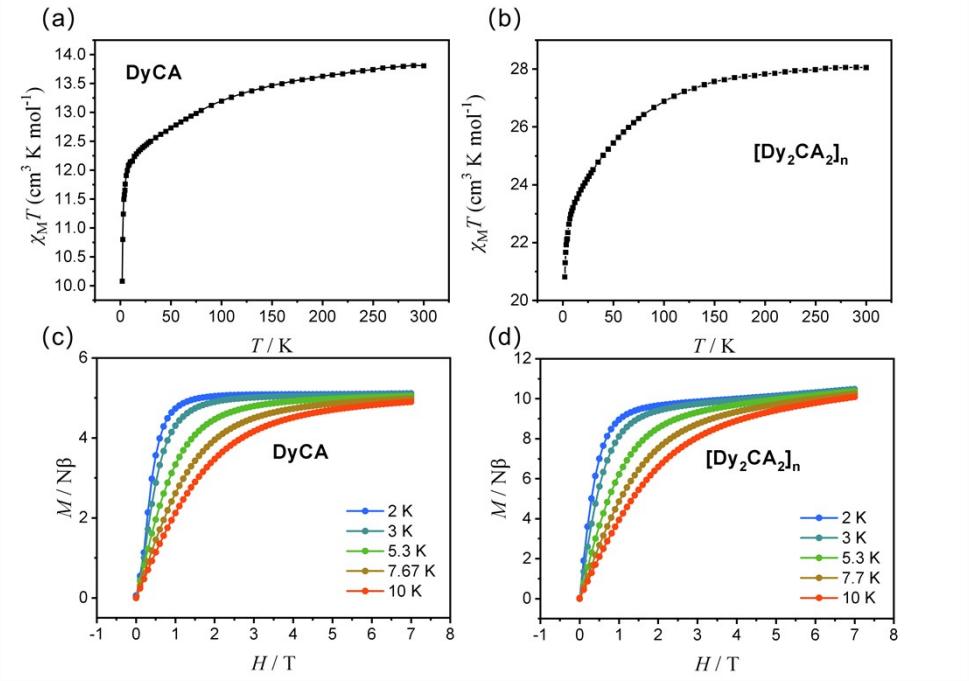

Fig. S6 (a, b) Temperature dependence of $\chi_M T$ measured at 1 kOe for **DyCA** (a) and **[Dy$_2$CA$_2$]$_n$** (b) on powder sample. (c, d) Field dependence of magnetization at 2-10 K for **DyCA** (c) and **[Dy$_2$CA$_2$]$_n$** (d) on powder sample.

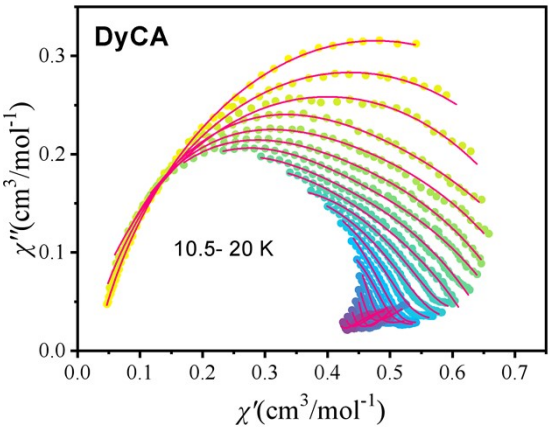

Fig. S7 Fitting result of Cole–Cole plots at 10.5–20 K of **DyCA** under 0 Oe DC field.

Table S5 Cole-Cole plot fitting parameters for **DyCA**.

T (K)	$\chi_{s(total)}$ (cm^3 mol^{-1})	χ_1 (cm^3 mol^{-1})	τ_1 (s)	α_1	χ_2 (cm^3 mol^{-1})	τ_2 (s)	α_2
10.5	0.02761	0.88963	6.26446E-4	0.21705	0.00763	1.10586E-4	0.04795
11	0.01423	0.83271	3.68235E-4	0.24635	0.01188	1.13254E-4	3.04923E-4
11.5	1.40916E-11	0.78776	2.14523E-4	0.27375	0.01795	7.72217E-5	5.02433E-4
12	1.18584E-10	0.61031	2.31941E-4	0.38372	0.203	6.53785E-5	0.00317
12.5	1.18795E-10	0.57907	1.43688E-4	0.36392	0.1875	3.53666E-5	0.0056
13	1.7025E-10	0.53128	9.91845E-5	0.36615	0.19913	2.15039E-5	0.00545
13.5	2.24893E-10	0.50419	7.36977E-5	0.40356	0.21052	1.51855E-5	0.00998
14	3.35331E-10	0.46419	4.61137E-5	0.38574	0.21004	9.54953E-6	0.02551
14.5	4.06299E-10	0.44768	2.6963E-5	0.42259	0.20238	7.78324E-6	0.07733

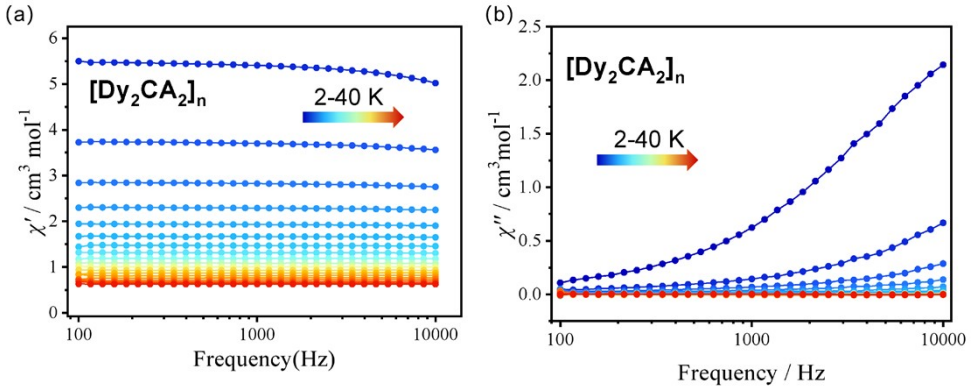

Fig. S8 AC magnetic susceptibility measurements of **$[Dy_2CA_2]_n$** under 0 Oe. Frequency dependence of the in-phase χ' (a) and out-of-phase χ'' (b) under a 0 Oe DC field in the range of 2-40 K. Solid lines served as guides.

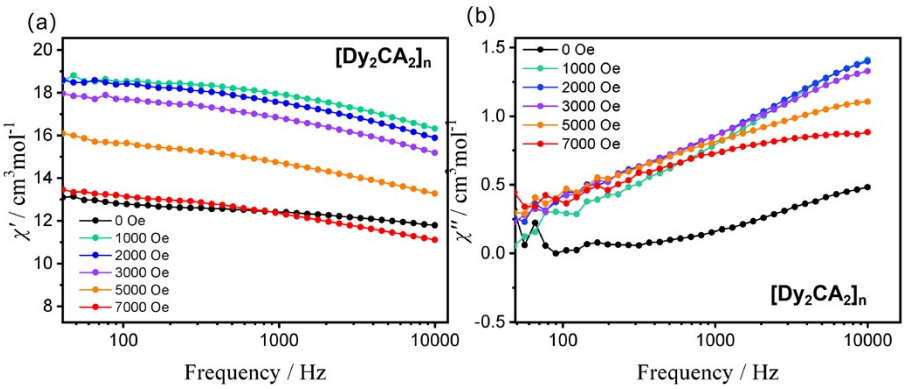

Fig.S9 Optimization field measurements of **$[Dy_2CA_2]_n$** under 0-7000 Oe DC field.

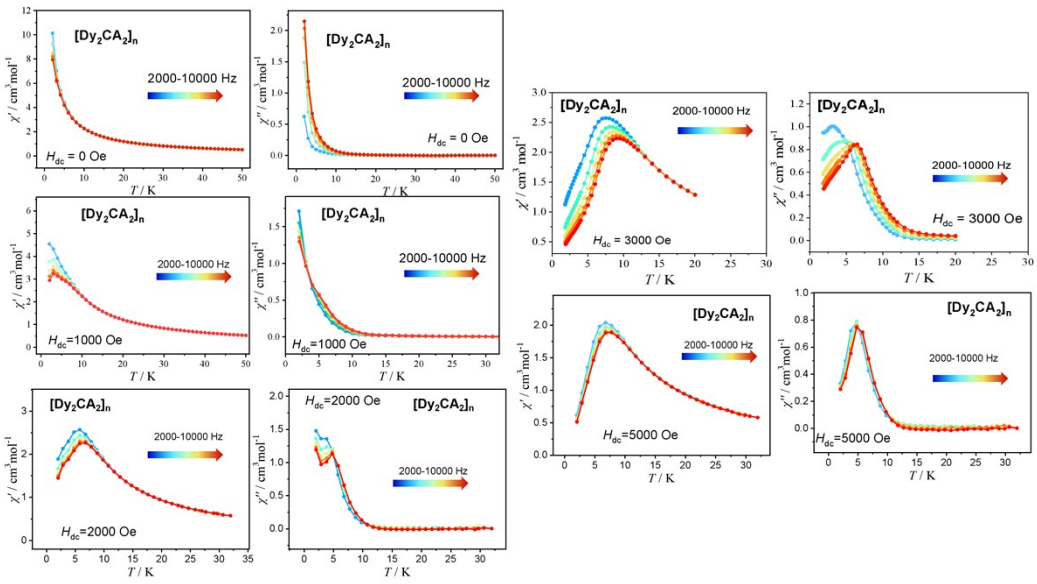

Fig. S10 Temperature-dependent AC magnetic susceptibility measurements of **$[Dy_2CA_2]_n$** under 0-5000 Oe DC field.

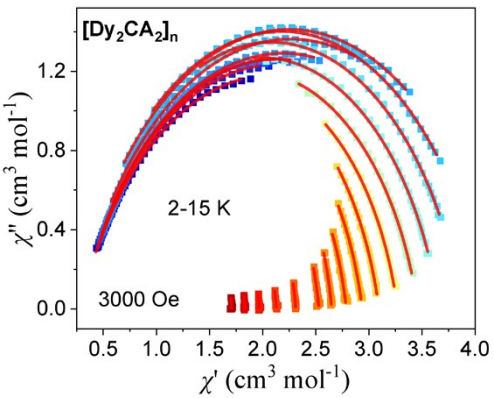

Fig. S11 (a) Fitting result of Cole–Cole plots at 2–15 K of **$[Dy_2CA_2]_n$** under 3000 Oe DC field.

Table S6 Cole-Cole plot fitting parameters for **$[Dy_2CA_2]_n$** under 3000 Oe DC field.

T (K)	χ_s ($cm^3\ mol^{-1}$)	χ_t ($cm^3\ mol^{-1}$)	τ (s)	α
2	0.27865	3.87091	3.90194E-4	0.26124
2.5	0.29622	3.92946	3.3743E-4	0.24143
3	0.29877	3.95829	2.96596E-4	0.23203
3.5	0.28797	4.00107	2.61337E-4	0.23994
4	0.28542	4.10216	2.20835E-4	0.24281
4.5	0.2694	4.26245	1.66302E-4	0.2376
5	0.24799	4.25947	1.00324E-4	0.21942
5.5	0.25228	4.10479	5.43182E-5	0.19927
6	0.2894	3.88063	2.95544E-5	0.1809
6.5	0.34279	3.6648	1.71172E-5	0.17013
7	0.35728	3.46493	1.03498E-5	0.16528
7.5	0.33658	3.2724	6.55453E-6	0.15168
8	0.04864	3.09804	3.75633E-6	0.15094
8.5	2.0085E-12	2.94017	2.51472E-6	0.1401
9	2.79555E-12	2.79038	1.8003E-6	0.12371
9.5	4.67184E-12	2.65329	1.40543E-6	0.09838
10	5.21196E-12	2.53215	1.01928E-6	0.10025

Table S7 The best fitting results of the temperature dependent relaxation times of **$[Dy_2CA_2]_n$** under 3000 Oe DC field.

$\tau^{-1} = \tau_{QTM}^{-1} + CT^n$	
τ_{QTM}^{-1}	2846.74895
C	0.08901
n	7.10371
Dominated relaxation processes	Raman and QTM

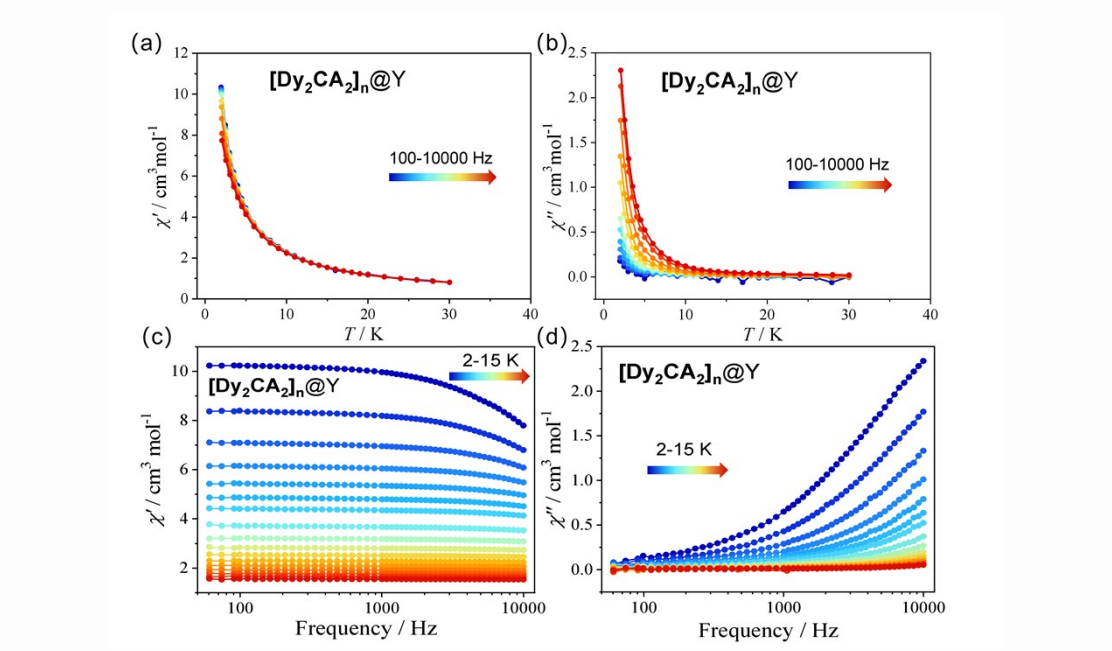

Fig. S12 AC magnetic susceptibility measurements of **[Dy_2CA_2]$_n$**@Y. Variable temperature magnetic susceptibility of the in-phase χ' (a) and out-of-phase χ'' (b) under a 0 Oe DC field. Variable frequency magnetic susceptibility of the in-phase χ' (c) and out-of-phase χ'' (d) under a 0 Oe DC field. Solid lines served as guides.

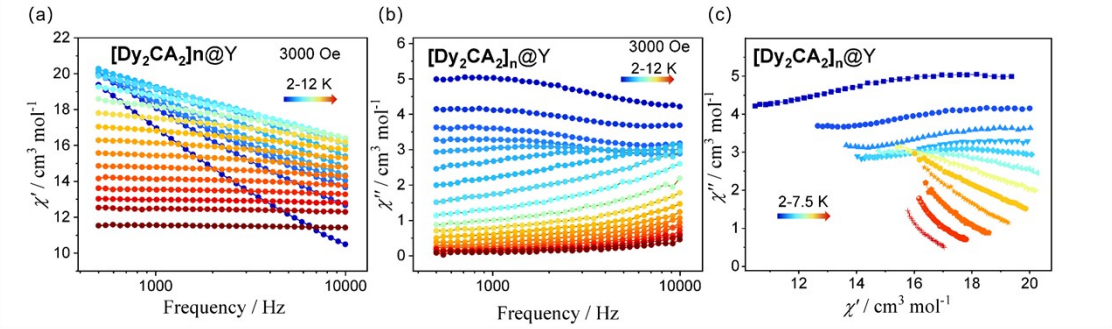

Fig. S13 AC magnetic susceptibility measurements of **[Dy_2CA_2]$_n$**@Y. Frequency dependence of the in-phase χ' (a) and out-of-phase χ'' (b) under 3000 Oe DC field in the range of 2-12 K. Solid lines served as guides. (c) Cole–Cole plots at 2–7.5 K of **[Dy_2CA_2]$_n$**@Y under 3000 Oe DC field.

The Lorentz function is selected as the peak type fitting model for multi-peak fitting. The fitting process was completed in the Origin software, using the Peak Analyzer tool in the Analysis window, and the Lorentz function is selected as the peak type fitting model for multi-peak fitting. The results fitted by Lorentz function are in good agreement with the total fitting curves. The goodness-of-fit coefficient (R^2) of each sub-peak (for the frequencies 4000, 5000, 6000, 7000, 8000, and 10000 Hz) are 0.9996,0.9995,0.9998,0.9998,0.9994, and 0.9996, respectively.

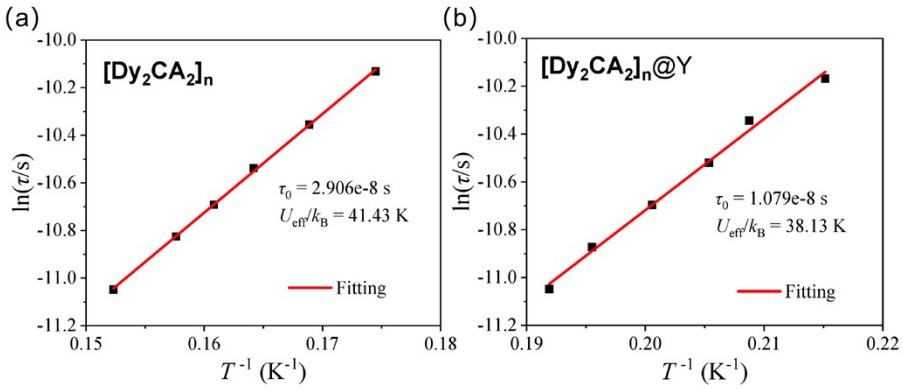

Fig. S14 The fitting energy barrier of the Orbach process fitted by the χ''-T plots. (a) Plots of ln(τ) *vs*. T^{-1} of **[Dy$_2$CA$_2$]$_n$** (3000 Oe). (b) Plots of ln(τ) *vs*. T^{-1} of **[Dy$_2$CA$_2$]$_n$**@Y (3000 Oe).

3. Computational details

Complete-active-space self-consistent field (CASSCF) calculations on individual Dy^{III} fragments for complexes **DyCA** and **$[Dy_2CA_2]_n$** have been carried out with the OpenMolcas program package. Considering the large structure of complex **$[Dy_2CA_2]_n$**, we simplify them to only include one Dy^{III} fragment shown in Figure S13b. Each individual Dy^{III} fragment was calculated keeping the experimentally determined structure of the corresponding compound. The basis sets for all atoms are atomic natural orbitals from the ANO-RCC library: ANO-RCC-VTZP for Dy(III); VTZ for close O and P; VDZ for distant atoms. The calculations employed the second order Douglas-Kroll-Hess Hamiltonian, where scalar relativistic contractions were taken into account in the basis set and the spin-orbit couplings were handled separately in the restricted active space state interaction (RASSI-SO) procedure. Active electrons in 7 active orbitals include all *f* electrons (CAS (9 in 7) in the CASSCF calculation. To exclude all the doubts, we calculated all the roots in the active space. We have mixed the maximum number of spin-free state which was possible with our hardware. SINGLE_ANISO program was used to obtain the energy levels, ***g*** tensors, magnetic axes, *etc.* based on the above CASSCF/RASSI-SO calculations.

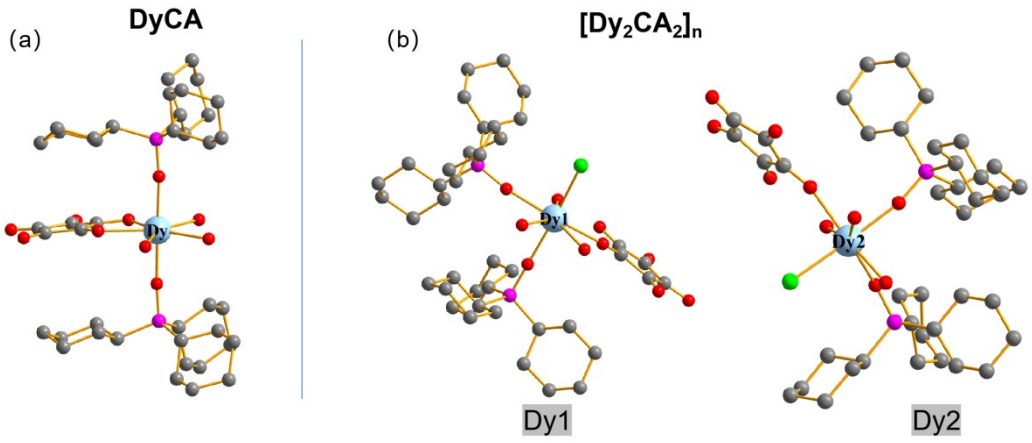

Fig. S15 Calculated molecular structures of complexes **DyCA** (a) and **$[Dy_2CA_2]_n$** (b); H atoms are omitted for clarify.

Table S8 Calculated energy levels (cm^{-1}), $\boldsymbol{g}$ (g_x, g_y, g_z) tensors and predominant m_J values of the lowest eight Kramers doublets (KDs) of individual Dy(III) fragments of **DyCA** and **$[Dy_2CA_2]_n$** using CASSCF/RASSI-SO with the OpenMolcas.

KDs	**DyCA**			**$[Dy_2CA_2]_n$_Dy1**			**$[Dy_2CA_2]_n$_Dy2**		
	E	***g***	m_J	*E*	***g***	m_J	*E*	***g***	m_J
0	0.0	0.000 0.000 19.867	±15/2	0.0	0.000 0.001 19.866	±15/2	0.0	0.013 0.031 19.527	±15/2
1	306.0	0.030 0.234 16.747	±13/2	334.6	0.095 0.123 16.956	±3/2	72.1	0.018 0.049 19.044	
2	340.4	0.498 0.784 18.538	±1/2	517.3	1.375 3.064 14.998	±13/2	189.6	0.355 0.466 14.629	
3	411.6	2.132 2.473 14.225		561.2	8.021 6.714 2.416		258.6	1.768 2.526 10.903	
4	478.0	2.917 5.134 9.346		596.6	0.233 4.351 9.414		333.0	3.183 4.807 9.178	
5	492.9	1.542 3.154 13.229		636.5	2.065 3.104 13.011		371.0	1.085 4.223 11.521	
6	559.3	1.342 2.914 13.520		674.3	3.796 6.335 10.328		431.2	1.476 4.572 9.937	
7	585.5	1.110 3.623 15.414		709.9	0.874 1.886 15.993		453.9	1.058 6.325 12.192	

Table S9 Wave functions with a definite projection of the total moment | m_J > for the lowest eight KDs of individual Dy(III) fragments of **DyCA** and **$[Dy_2CA_2]_n$** using CASSCF/RASSI-SO with the OpenMolcas.

	KDs	E/cm^{-1}	wave functions
DyCA	0	0.0	99.9%|±15/2>
	1	306.0	96.7%|±13/2>
	2	340.4	65.7%|±1/2>+25.1%|±3/2>
	3	411.6	49.2%|±3/2>+17%|±5/2>+14%|±1/2>+11.4%|±7/2>
	4	478.0	53.2%|±11/2>+20.7%|±5/2>+8.4%|±7/2>+7.7%|±9/2>
	5	492.9	38.7%|±5/2>+24.8%|±11/2>+15.3%|±1/2>+13.2%|±3/2>
	6	559.3	51.6%|±7/2>+25.1%|±9/2>+13.7%|±11/2>
	7	585.5	57.6%|±9/2>+25.2%|±7/2>+9.7%|±5/2>
	4	246.3	27.6%|±13/2>+23.4%|±5/2>+22.3%|±11/2>+11.8%|±7/2>+4.9%|±3/2>
	5	323.1	37.7%|±9/2>+31.1%|±11/2>+15.9%|±7/2>+7.5%|±13/2>
	6	347.8	32.4%|±5/2>+29.1%|±3/2>+17.4%|±7/2>+9.1%|±1/2>+4.9%|±9/2>
	7	385.2	24.1%|±9/2>+21.6%|±7/2>+21.1%|±1/2>+13.2%|±11/2>+9.2%|±5/2>+8.7%|±3/2>
$[Dy_2CA_2]_n$ _Dy1	0	0.0	95.7%|±15/2>
	1	334.6	26.9%|±3/2>+26.2%|±1/2>+21.6%|±5/2>+12.4%|±7/2>+6%|±9/2>
	2	517.3	54.1%|±13/2>+19.3%|±1/2>+10%|±9/2>+6%|±3/2>+4.8%|±7/2>
	3	561.2	34.6%|±13/2>+25.8%|±1/2>+11.1%|±7/2>+9.8%|±5/2>+8.8%|±3/2>
	4	596.6	41.6%|±3/2>+24.7%|±11/2>+15%|±1/2>+7.6%|±9/2>+3.9%|±13/2>
	5	636.5	38.5%|±11/2>+35.1%|±5/2>+11.8%|±3/2>+10.6%|±1/2>
	6	674.3	29.2%|±9/2>+26.5%|±5/2>+20.3%|±7/2>+19.2%|±11/2>
	7	709.9	46.1%|±7/2>+43.4%|±9/2>
$[Dy_2CA_2]_n$ _Dy2	0	0.0	95%|±15/2>
	1	72.1	46.6%|±1/2>+30.1%|±3/2>+13.8%|±5/2>
	2	189.6	23.8%|±7/2>+23.2%|±3/2>+16.2%|±13/2>+12.8%|±7/2>+10.6%|±1/2>+10%|±9/2>
	3	258.6	61.3%|±13/2>+13.6%|±3/2>+13.4%|±1/2>+4.5%|±7/2>
	4	333.0	31.9%|±5/2>+17.3%|±1/2>+16.1%|±7/2>+12%|±11/2>+10.9%|±13/2>+9.9%|±3/2>
	5	371.0	24.9%|±11/2>+20.2%|±7/2>+17.2%|±3/2>+13%|±5/2>+10.7%|±9/2>+8.1%|±1/2>
	6	431.2	38.8%|±11/2>+33.3%|±9/2>+14.7%|±7/2>+5.2%|±5/2>
	7	453.9	40.1%|±9/2>+26.5%|±7/2>+16.5%|±11/2>+10.9%|±5/2>

To fit the exchange interactions of the Dy(III)-Dy(III) in **[Dy$_2$CA$_2$]$_n$**. we took two steps to obtain them. Firstly, we calculated individual Dy(III) fragments using CASSCF/RASSI-SO to obtain the corresponding magnetic properties. Then, the exchange interactions between the magnetic centers were considered within the Lines model, which is effective and has been successfully used widely in the research field of d and *f*-elements single-molecule magnets.

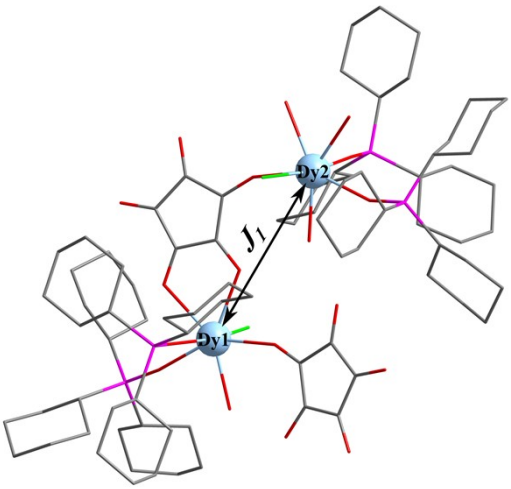

Figure S16. Scheme of the Dy(III)-Dy(III) interactions in **[Dy$_2$CA$_2$]$_n$**.

The Ising total Hamiltonians for **[Dy$_2$CA$_2$]$_n$** is $\hat{H}_{exch} = -\tilde{J}_1 \hat{S}_{Dy1} \hat{S}_{Dy2}$, where $\tilde{J}_1 = 25 J_1 \cos\theta$ is the parameters of the effective magnetic coupling constants for Dy(III)-Dy(III) with respect to the ground pseudospin of $\tilde{S}_{Dy} = 1/2$ on the Dy(III) site. The Lines exchange coupling constants J were fitted through comparison of the computed and measured magnetic susceptibilities using the POLY_ANISO program.

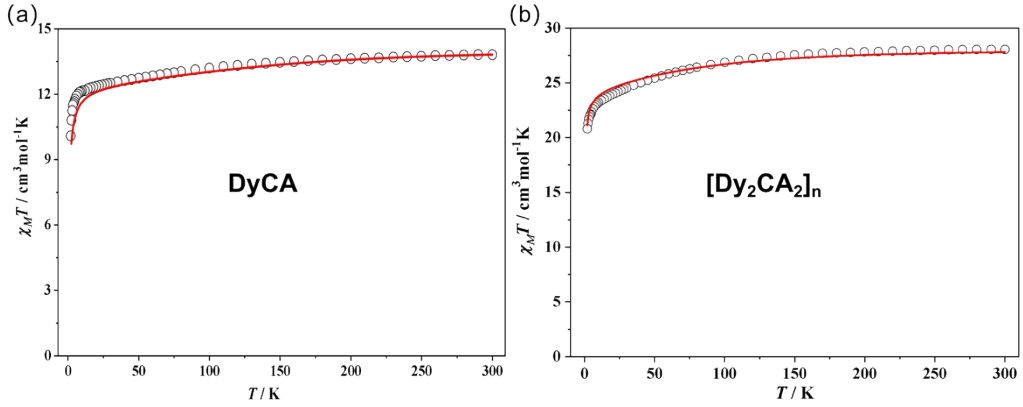

Figure S17. Calculated (red solid line) and experimental (black circle dot) data of magnetic susceptibilities of complex **DyCA** (a) and **[Dy$_2$CA$_2$]$_n$** (b), respectively. The intermolecular interactions zJ' of them were fitted to −0.08 and 0.01 cm^{-1}, respectively.

Table 10 Fitted exchange couplings $\tilde{J}_{exch}$, the calculated dipole-dipole interaction $\tilde{J}_{dip}$ and the total

constants J_{total} between Dy(III) in **[Dy$_2$CA$_2$]$_n$**. The intermolecular interactions zJ' of **DyCA** and **[Dy$_2$CA$_2$]$_n$** were fitted to −0.08 and 0.01 cm^{-1}, respectively.

	[Dy$_2$CA$_2$]$_n$		
	J_{exch}	J_{dip}	J_{total}
J_1	0.24	−0.47	−0.23

Table S11 Exchange energies E (cm^{-1}), the energy differences between each exchange doublet Δ_t (cm^{-1}) and the main values of the g_z for the lowest 2 exchange doublets arising from the exchange interactions on magnetic centers complex **[Dy$_2$CA$_2$]$_n$**, respectively.

	[Dy$_2$CA$_2$]$_n$		
Exchange doublets	E	Δ_t	g_z
0	0.000000000000	1.776×10^{-12}	6.020
	0.000004398201		
1	0.486716740516	1.875×10^{-10}	38.318
	0.486724598959		